Substrate recognition by a carbohydrate-binding module in the prototypical ABC transporter for lipopolysaccharide O-antigen from *Escherichia coli* O9a

Received for publication, July 25, 2019, and in revised form, August 14, 2019 Published, Papers in Press, August 15, 2019, DOI 10.1074/jbc.RA119.010323

Evan Mann[‡1,2], **Steven D. Kelly**[‡1,3], **M. Sameer Al-Abdul-Wahid**[§], **Bradley R. Clarke**[‡], **Olga G. Ovchinnikova**[‡], **Bin Liu**[¶], **and Chris Whitfield**[‡4]

From the [‡]*Department of Molecular and Cellular Biology and the* [§]*Advanced Analysis Centre, University of Guelph, Guelph, Ontario N1G 2W1, Canada and the* [¶]*TEDA Institute of Biological Sciences and Biotechnology, Nankai University, 3 Hongda St. TEDA, Tianjin 300457, China*

Edited by Gerald W. Hart

Escherichia coli **serotype O9a provides a model for export of lipopolysaccharide (LPS) O-antigen polysaccharide (O-PS) via ABC transporters. In O9a biosynthesis, a chain-terminator enzyme, WbdD, caps the nonreducing end of the glycan with a methylphosphate moiety and thereby establishes chain-length distribution. A carbohydrate-binding module (CBM) in the ABC transporter recognizes terminated glycans, ensuring that only mature O-PS is exported and incorporated into LPS. Here, we addressed two questions arising from this model. Are both residues in the binary terminator necessary for termination and export? And is a terminal methylphosphate moiety sufficient for export of heterologous glycans? To answer the first question, we uncoupled WbdD kinase and methyltransferase activities. WbdD mutants revealed that although the kinase activity is solely responsible for chain-length regulation, both activities are essential for CBM recognition and export. Consistent with this observation, a saturation transfer difference NMR experiment revealed a direct interaction between the CBM and the terminal methyl group. To determine whether methylphosphate is the sole determinant of substrate recognition by the CBM, we exploited *Klebsiella pneumoniae* O7, whose O-PS repeat-unit structure differs from O9a, but, as shown here, offers the second confirmed example of a terminal methylphosphate serving in substrate recognition. *In vitro* and *in vivo* experiments indicated that each CBM can bind the O-PS only with the native repeat unit, revealing that methylphosphate is essential but not sufficient for substrate recognition and export. Our findings provide important new insight into the structural determinants in a prototypical quality control system for glycan assembly and export.**

This research was supported by funding from the Natural Sciences and Engineering Research Council of Canada (to C. W.). The authors declare that they have no conflicts of interest with the contents of this article.
This article contains Table S1 and Figs. S1–S4.

[1] Both authors contributed equally to this work.
[2] Recipient of an Alexander Graham Bell Canada Graduate Scholarship from the Natural Sciences and Engineering Research Council of Canada.
[3] Recipient of an Alexander Graham Bell Postgraduate Scholarship Doctoral award from the Natural Sciences and Engineering Research Council of Canada.
[4] Recipient of a Canada Research Chair. To whom correspondence should be addressed: Dept. of Molecular and Cellular Biology, University of Guelph, 50 Stone Rd. East, Guelph, Ontario N1G 2W1, Canada. Tel.: 519-824-4120 (ext. 53361); E-mail: cwhitfie@uoguelph.ca.

Lipopolysaccharide (LPS)[5] is the major glycolipid of the Gram-negative bacterial outer membrane (1). It is almost always essential for cellular viability and is important for pathogenicity. The tripartite structure of LPS consists of the outer membrane–embedded component, lipid A (also known as endotoxin), a core oligosaccharide, and a structurally variable and immunogenic sugar polymer termed O-antigen (O-PS) (2). In human pathogens, O-PS is one of the first molecules encountered by the host, and it provides protection to the bacterium from immune processes such as the complement system (3). For resistance to serum killing, the length of the O-PS is a critical factor in promoting a successful defense, with longer O-PS providing a more effective barrier (4, 5). Loss of O-PS chain-length regulation has resulted in loss of serum resistance and susceptibility to leukocytes in some Gram-negative bacteria (5). There are many different O-PS structures with the diversity driven by selective environmental factors, such as host immune response and bacteriophages that exploit O-PSs as receptors (6).

Many O-PSs are assembled by a mechanism that requires an ATP-binding cassette (ABC) transporter to export lipid-linked O-PS intermediates from the site of synthesis in the cytosol to the periplasm (7, 8), where the LPS molecule is completed before being translocated to the cell surface by the Lpt (LPS transport) machinery (9, 10). The ABC transporter provides an important role in determining the chain-length distribution of the O-PS products, with two main mechanisms being described. In the simpler process exhibited by *Klebsiella pneumoniae* serotype O2a (11), the O-PS is polymerized to completion within the cytosol by a biosynthetic enzyme complex. The chain-length distribution is controlled by the relative activities of a complex of glycosyltransferase (GT) enzymes and the ABC transporter. The O2a ABC transporter does not possess strict O-PS specificity, and it can export polymers with diverse

[5] The abbreviations used are: LPS, lipopolysaccharide; O-PS, O-antigeni polysaccharide; ABC, ATP-binding cassette; Lpt, LPS transport; GT, glycosyltransferase; CBM, carbohydrate-binding module; Und-P, undecaprenol phosphate; Kdo, 3-deoxy-D-*manno*-oct-2-ulosonic acid; STD, saturation transfer difference; STDD, saturation transfer double difference; COSY, correlation spectroscopy; TOCSY, total correlation spectroscopy; NOESY, nuclear Overhauser effect spectroscopy; HSQC, heteronuclear single-quantum coherence; HMBC, heteronuclear multiple-bond correlation; LB, lysogeny broth; Bis-Tris, 2-[bis(2-hydroxyethyl)amino]-2-(hydroxymethyl)propane-1,3-diol.

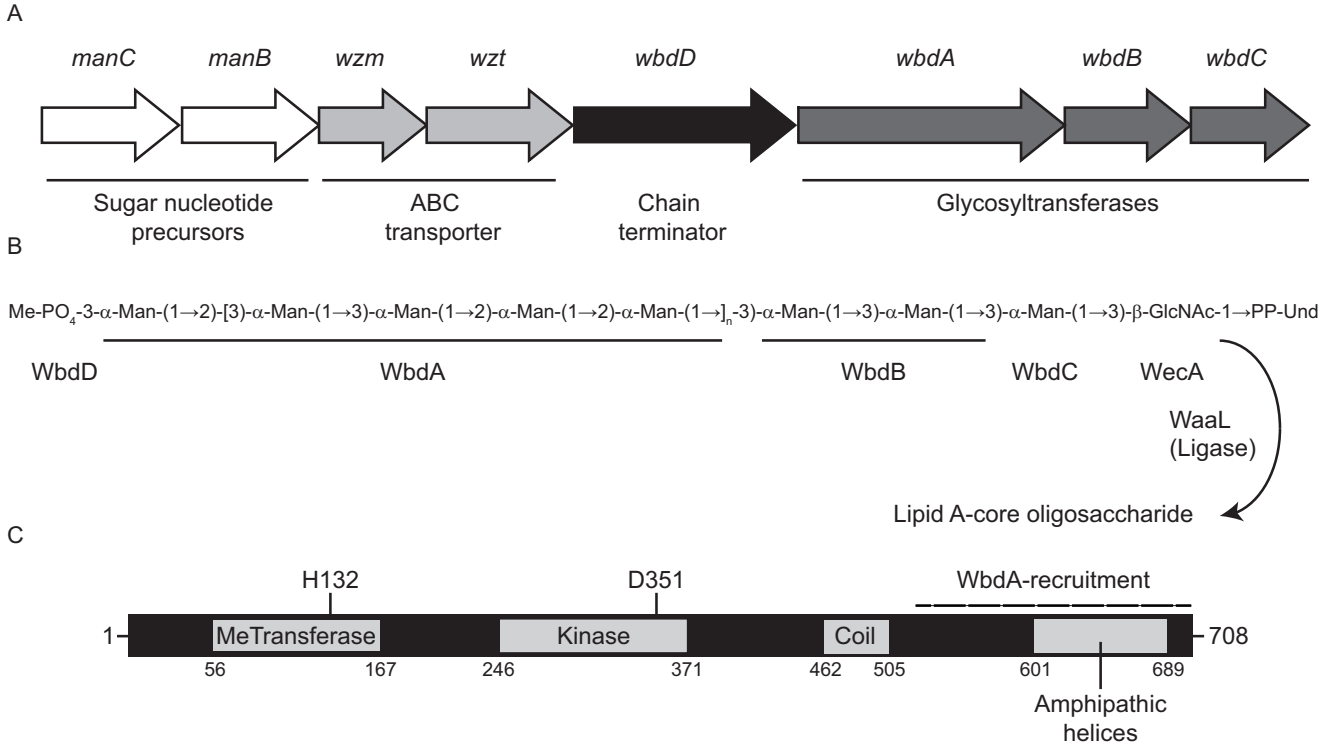

Figure 1. Structure and biosynthesis of the *E. coli* O9a O-PS. *A*, organization of the O-PS synthesis (*wb**) operon. *B*, structure of the Und-PP–linked O9a biosynthetic intermediate. The *square brackets* delineate the tetrasaccharide O-PS repeat unit. *Man*, D-mannose; GlcNAc, D-GlcNAc. *C*, domain organization of the dual kinase methyltransferase WbdD. The coiled-coil domain acts as a molecular ruler separating WbdA, which is recruited to its interaction site at the C terminus of WbdD (indicated), from the chain-terminating catalytic sites of WbdD.

repeat-unit structures, but polymerization and export are obligatorily coupled (11, 12). The more intricate *Escherichia coli* serotype O9a O-PS assembly system incorporates an additional mechanism that imposes a stricter level of control over chain length. This requires the installation of a chain-terminating residue that creates an export signal recognized by a carbohydrate-binding module (CBM) attached to the ABC transporter. In this system, polymerization and export can be temporally uncoupled *in vitro* (11). The structural requirements for glycan recognition by the CBM provide the focus of this study.

During O-PS biosynthesis in both systems, the 55-carbon polyisoprene carrier lipid, undecaprenol phosphate (Und-P) serves as the acceptor for the shared initiating phosphoglycosyltransferase enzyme, named WecA (2). In serotype O9a, the resulting Und-PP-GlcNAc product is then extended by serotype-specific mannosyltransferases to create the O9a O-PS backbone (Fig. 1). Central to polymerization is WbdA, a dual-domain GT polymerase that catalyzes formation of alternating pairs of α1–2- and α1–3-linkages (13, 14). WbdA operates in a distributive (rather that processive) manner, where the growing chain is released from the enzyme at each step (14, 15). The length of the O9a O-PS is dictated by WbdD. The C terminus of WbdD contains a membrane-anchoring helix and a region that recruits WbdA into an active membrane-bound heterocomplex (Fig. 1*C*) (14, 16). The N terminus of WbdD possesses kinase and methyltransferase catalytic sites that add a phosphomethyl moiety to the nonreducing terminus of the O-PS, blocking further extension by WbdA (17–19). The physical separation of the chain-terminating domain from the membrane by an extended coiled-coil ensures that only O-PS of a minimum length can be capped (20). In addition to operating as a molecular ruler, the coiled-coil structure facilitates multimerization of functional WbdD trimers. The relative abundance of WbdA and WbdD also affects the distribution of O-PS lengths, and this is explained by the variable geometry model that describes the outcome of changes in the stoichiometries of the WbdA-WbdD heterocomplexes (21).

Essential to this chain-length regulation strategy is a quality control mechanism on the ABC transporter protein complex, which ensures that only terminated (and chain-regulated) O-PS is exported for assembly on the cell surface. O-PS ABC transporters are composed of homodimers of the transmembrane domain protein (Wzm) and the nucleotide-binding domain protein (Wzt). In *E. coli* O9a and related assembly systems, Wzt possesses a C-terminal CBM, which is specific for its cognate O-PS (12, 22, 23). Binding of O-PS by the CBM is a prerequisite for transport, and removal or mutation of the CBM abrogates export (23). The *Aquifex aeolicus* Wzm-Wzt ABC transporter is currently the only solved structure for this class of exporter, and it shares similarity with *E. coli* O9a Wzm-Wzt (24). Although the *A. aeolicus* structure was solved without the cognate CBM, it has allowed the development of mechanistic models for O-PS transport. Key mechanistic predictions were tested by examining the phenotypes of the corresponding mutations in *E. coli* O9a Wzm-Wzt. *In vitro* data shows that the CBM stimulates ATP turnover by Wzm-Wzt in proteoliposomes (24), suggesting a more complex role that is not confined

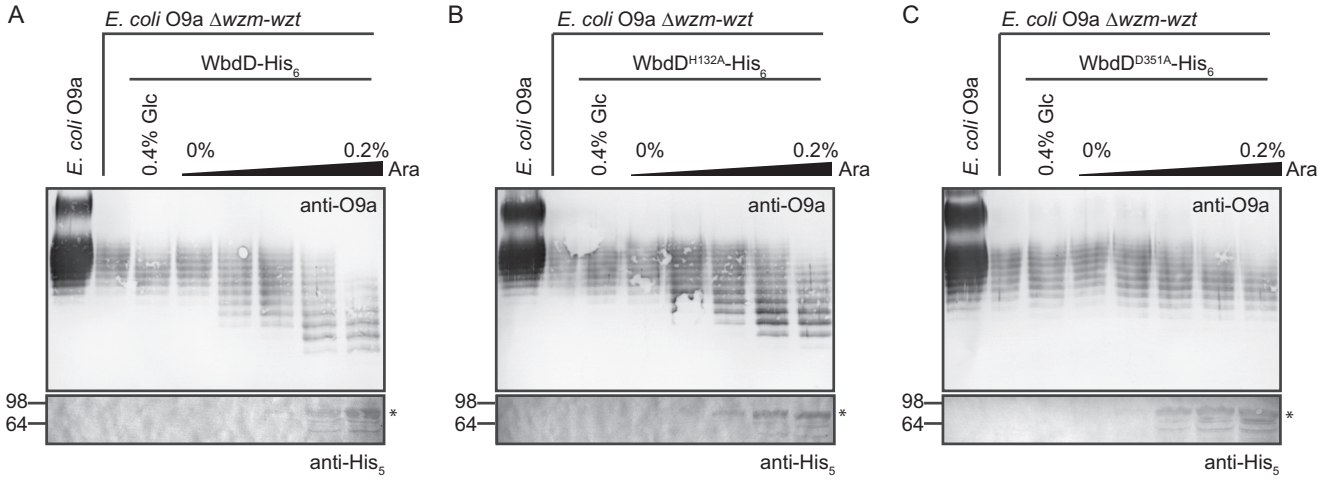

Figure 2. The kinase domain of WbdD is sufficient for chain termination *in vivo*. Levels of WbdD-His_6 (expressed from pWQ470) (*A*) and its mutants with inactivated methyltransferase (His^{132} → Ala; pWQ829) (*B*) or kinase (Asp^{351} → Ala; pWQ830) (*C*) catalytic sites were titrated in *E. coli* CWG638 *manA* Δ*wzm-wzt*::*aphA-3*. The addition of 0.4% D-glucose was used to repress the pBAD promoter, whereas varying concentrations of L-arabinose induced expression of the WbdD variants. To overcome second site mutations occurring during prolonged growth in the absence of functional O-PS export (17), a *manA* mutant was used, making O9a O-PS biosynthesis conditional on the addition of mannose to the growth medium at the beginning of the experiment. Und-PP–linked O-PS intermediates (accumulating in the absence of transport) were detected in proteinase K–digested whole-cell lysates by SDS-PAGE and immunoblotting with O9a-specific antibodies (*top panels*). The control lane is authentic O9a LPS from the *manA* strain (CWG634). The *bottom panels* show the detection of WbdD-His_6 variants by immunoblotting with anti-His_5 antibodies.

to substrate recognition. Notably, constructs where the O9a CBM and nucleotide-binding domain are artificially separated retain export function *in vivo* (23).

Similar chain termination/export strategies exist in other species and/or serotypes. For example, O-PS chain regulation is achieved by the addition of a methyl group in *E. coli* O8 or a sugar (3-deoxy-D-*manno*-oct-2-ulosonic acid; Kdo) in *K. pneumoniae* O12 (25). The involvement of both phosphate and methyl residues in chain-length regulation in *E. coli* O9a appears unnecessarily complicated; in principle, a single terminating residue should suffice. Given the pivotal role the *E. coli* O9a O-PS system plays as an influential prototype for bacterial glycan export, it is essential to understand the details and limitations of substrate recognition and export. This provides the goal of the current study.

Results

WbdD kinase activity is solely responsible for arresting O9a O-PS polymerization

The modal distribution of O9a-PS chain lengths is established by the coiled-coil domain, which physically separates the WbdD termination enzymes from membrane-anchored WbdA (20). Previous work established that WbdD halts WbdA-mediated O-PS extension by installation of a phosphomethyl moiety to the nonreducing terminus, where new backbone residues are added (17, 20, 21). Logically, the addition of a single terminating residue to the site of O-PS extension should be sufficient for regulation of chain-length distribution. To confirm this hypothesis and rule out any unanticipated requirements for a functional methyltransferase, we exploited the observation that overexpression of a functional WbdD terminator decreases the average chain length of O-PS (21). Mathematical modeling supports the hypothesis that O-PS chain length responds to altered stoichiometry within the WbdA:WbdD heterocomplex, with the resulting changes in geometry of the complex altering access of the glycan to termination catalytic sites (21). The O-PS phenotype is readily assessed by SDS-PAGE profiles of Und-PP–linked O9a intermediates in whole-cell lysates. These intermediates are not visible in silver-stained SDS-PAGE but are readily visualized in immunoblots using O-PS–specific antibodies (11, 12, 26).

These experiments were performed in a *manA* Δ*wzm-wzt*::*aphA-3* background, where O-PS production is conditionally dependent on the addition of D-mannose to the growth medium (17). This is necessary to avoid any unexpected effects on viability of the transformants, known to occur when O9a export is eliminated (22). After SDS-PAGE of whole-cell lysates, O9a intermediates were detected using O9a-specific antibodies (Fig. 2). Prior *in vitro* experiments verified that $WbdD^{H132A}$ and $WbdD^{D351A}$ lack methyltransferase and kinase activities, respectively (19). Each variant was expressed from a pBAD promoter by titrating the L-arabinose inducer, and the expected increase in protein production was confirmed by exploiting the His_6 tag for Western immunoblotting. As shown previously (21), increasing levels of WT WbdD resulted in an inducer-dependent reduction in the average O-PS intermediate chain-length (Fig. 2*A*). The profiles of O9a intermediates in cells overexpressing the methyltransferase mutant ($WbdD^{H132A}$) were qualitatively similar to those with WT WbdD (Fig. 2*B*). In contrast, the kinase mutant ($WbdD^{D351A}$) had no effect on the chain-length distribution of O-PS intermediates (Fig. 2*C*). These results show that the addition of the activity of the kinase is sufficient to determine O-PS chain length *in vivo* and that the kinase and methyltransferase activities can be uncoupled.

The terminating methyl group is essential for export by Wzm-Wzt

To evaluate whether O9a O-PS lacking normal nonreducing terminal modification could be transported across the inner

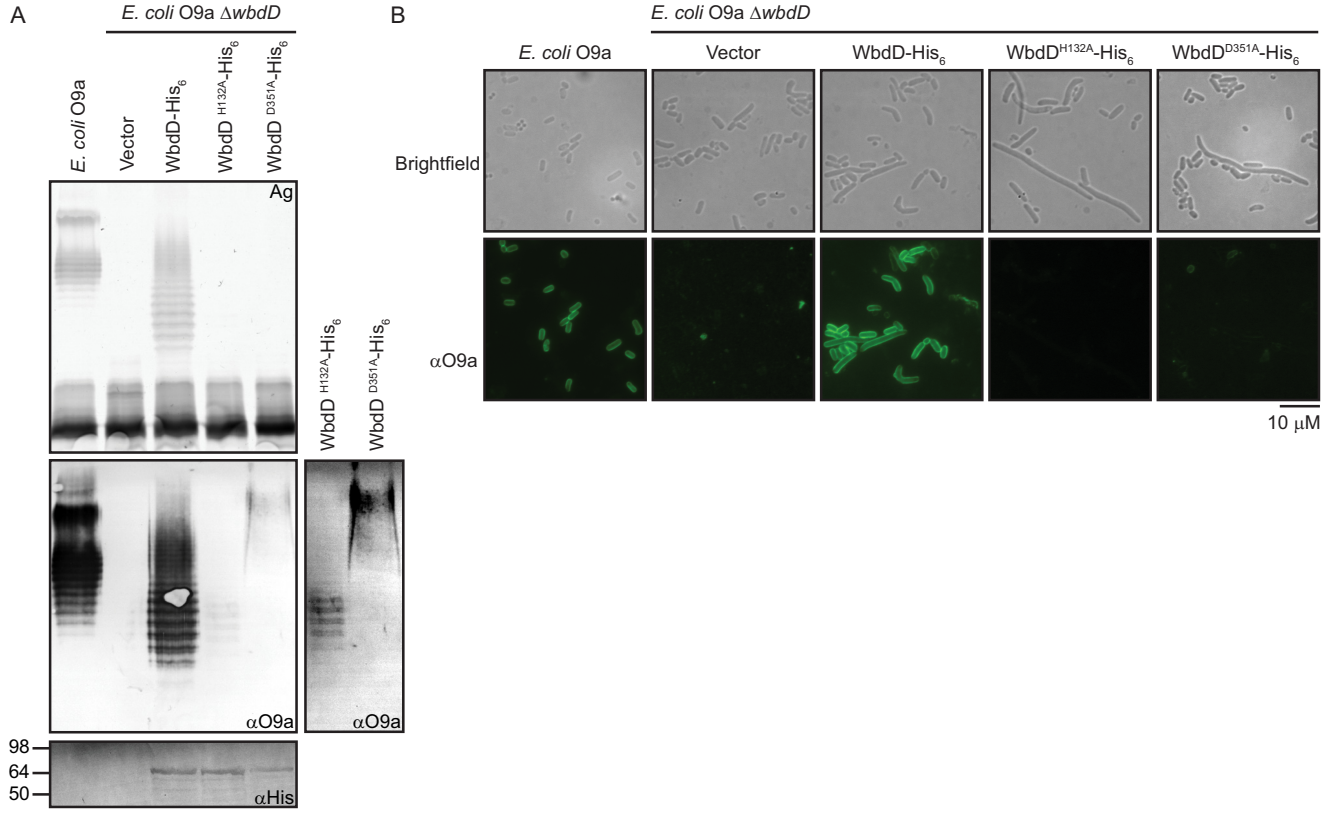

Figure 3. The complete O-antigen–terminating moiety is essential for export of O9a O-PS and cell-surface exposure. *E. coli* O9a *manA* Δ*wbdD* (CWG900) cells were transformed with plasmids expressing WbdD-His_6 (pWQ470) and its variants, $WbdD^{H132A}$-His_6 (pWQ829) or $WbdD^{D351A}$-His_6 (pWQ830), and examined by SDS-PAGE and immunoblotting (*A*) or immunofluorescence microscopy (*B*). Protein expression was induced with 0.02% L-arabinose. *E. coli* O9a *manA* (CWG634) provided the positive control. *A*, the *top panel* displays the LPS profile of proteinase K–treated whole-cell lysates resolved by SDS-PAGE and stained with silver. The *middle panel* is an immunoblot using polyclonal primary antibodies directed against O9a (note that immunoblotting detects both Und-PP-linked and lipid A-linked O-PS). Due to the high signal from complete LPS compared with Und-PP–linked intermediates in equivalent amounts of cells, a longer exposure of the lanes containing the Und-PP–linked intermediates is shown on the *right*. The *bottom panel* is a Western immunoblot using antibodies directed against the C-terminal His_6 tags on WbdD to confirm protein expression. *B*, immunofluorescence microscopy of the corresponding cells, using O9a-specific antibodies to detect surface-exposed O9a O-PS. Brightfield and immunofluorescence microscopy experiments were performed on formalin-fixed whole cells, probed with an anti-O9a rabbit antiserum and an FITC-conjugated secondary antibody.

membrane, an *E. coli* O9a *manA* Δ*wbdD* mutant was transformed with plasmids expressing the WbdD mutant variants. Export activity was monitored by silver-stained LPS profiles in whole-cell lysates separated by SDS-PAGE (Fig. 3*A*). Whereas plasmids expressing WT WbdD restored the production of O-PS– containing LPS visible in silver-stained gels, only O-PS–deficient LPS was evident in cells expressing either $WbdD^{H132A}$ or $WbdD^{D351A}$. However, as expected, small amounts of Und-PP–linked O-PS were still detected by Western immunoblotting in cells expressing $WbdD^{H132A}$ or $WbdD^{D351A}$. Whereas the $WbdD^{H132A}$ variant produced a banding pattern resembling the O-PS chain-length profile of the WT LPS, the $WbdD^{D351A}$ O-PS was of a higher molecular weight, as anticipated from the lack of chain-length regulation described above.

To confirm export status, immunofluorescence microscopy was performed to determine whether O-PS was present on the cell surface of the transformed mutants. O-PS was probed with a primary antiserum directed against the O9a antigen and a secondary antibody conjugated with FITC (Fig. 3*B*). Images of the parent O9a strain and the *manA* Δ*wbdD* mutant transformed with the WT *wbdD* gene displayed robust signal from surface-exposed O9a O-PS. In contrast, *manA* Δ*wbdD* cells transformed with vector or either mutant *wbdD* gene generated no immunofluorescence, consistent with the data in Fig. 3*A*. Brightfield images show that cells accumulating intracellular O-PS intermediates possess morphological defects (typically elongated cells), as reported previously (22). Taken together, these results indicated that the ABC transporter could not export either the nonmethylated O-PS or the nonterminated (nonphosphorylated and nonmethylated) O-PS.

The carbohydrate-binding module on Wzt is unable to recognize nonmethylated O9a O-PS

Previous work demonstrated that the C-terminal domain of Wzt functions as a CBM (23). In that study, an *in vitro* pulldown approach revealed the CBM binds its cognate O-PS, but not O-PS lacking the terminal methylphosphate or O-PS from *E. coli* O8 possessing a polymannose structure (with a repeat-unit structure different from that of O9a) capped with a terminal methyl group. To determine whether the requirement for O-PS methylation for export is dictated by the CBM-binding step, purified LPSs lacking either terminal phosphomethyl or methyl modifications were tested using the same pulldown approach. LPS molecules with chemically distinct nonreducing termini were generated using a strategy exploited previously to generate nonterminated *K. pneumoniae* O12 LPS (12). This

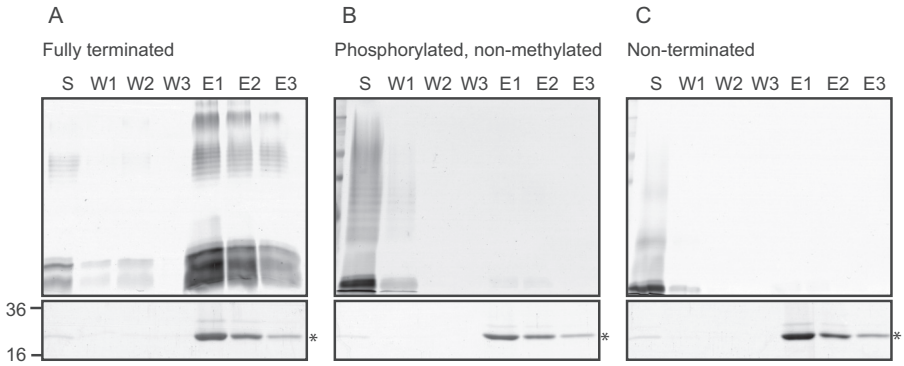

Figure 4. The Wzt CBM does not recognize nonmethylated LPS. Pulldown experiments were performed using purified *E. coli* O9a CBM (Wzt-C-His_6) and one of three LPS species: WT O9a (*A*), nonmethylated O9a (*B*), or nonterminated O9a (*C*). Reaction mixtures consisting of 200 μg of CBM and 200 μg of LPS were mixed with nickel magnetic beads and collected using a magnet. The samples are unbound material in the supernatant (*S*) and material released by sequential washes of the beads in the absence (*W1–W3*) or presence of imidazole (*E1–E3*). Aliquots of the collected samples were subjected to SDS-PAGE. LPS was detected by silver staining (*top panels*) and protein was detected by simply blue staining (*bottom panels*).

method takes advantage of the ability of the *K. pneumoniae* O2a ABC transporter to export heterologous O-PS intermediates. This transporter lacks a CBM and has no specificity for either the repeat-unit structure or terminal modifications of O-PS substrates (11, 27). It can therefore export LPS molecules with varying terminal modifications. LPS species were purified from *E. coli* O9a Δ*wbdD* transformed with plasmids to express the *K. pneumoniae* O2a transporter and appropriate WbdD variants.

The pulldown experiments follow retention (or not) of LPS by His_6-tagged CBM using nickel magnetic beads (Fig. 4). In the control experiments with WT O9a LPS, a considerable amount of LPS eluted in fractions containing CBM as reported previously (23). However, when CBM was incubated with either nonmethylated or nonmethylated/nonphosphorylated LPS, no binding was evident, indicating that the methyl group is essential for recognition by the CBM, and the phosphate group alone is insufficient. The inability of the CBM to bind improperly terminated O-PS is entirely consistent with the transport defects described above. These data support the notion that the impaired transport reflects altered substrate recognition but cannot exclude additional defects in later transport stages resulting from a terminally exposed phosphate.

Direct interaction between the nonreducing terminal methylphosphate and the CBM

During the characterization of the O9a CBM, residues in a putative binding pocket were identified that abrogated O-PS binding *in vitro* or had adverse effects on export *in vivo* (23). A saturation transfer difference (STD) NMR experiment (28) was used to provide more insight into the interaction and to formally verify the direct role of the methyl group in Wzt^{O9a}-C: O9a binding. Similar experiments have been performed previously to precisely define the interaction sites of antibodies with glycans by "epitope mapping" (*e.g.* see Refs. 29–31). The method relies on the application of precise radiofrequency pulses to selectively saturate the NMR signals of the protein; this saturation is then transferred to ligands that transiently bind the protein, attenuating the NMR signals of ligand protons at and near the binding site. To better observe small (>5%) attenuations, STD spectra are collected as the difference of an "on-resonance" spectrum (*i.e.* saturation pulses applied on the protein signals) and an "off-resonance" reference spectrum (*i.e.* saturation pulses applied far away from any NMR signals). STD spectra therefore display only signals corresponding to ligand protons that are at and near the protein-binding site. To address complications arising from saturation in the presence of larger ligands (30), a saturation transfer double difference spectrum (STDD) (32) is obtained by subtracting an STD spectrum obtained from a sample without protein from the protein-ligand STD spectra.

Serotype O9a O-PS was purified, and its structure was confirmed by comparison against the reported NMR data (13, 33) (data not shown). For STD NMR experiments, two samples were prepared. The first sample contained an approximately 100-fold excess of O9a polysaccharide mixed with Wzt^{O9a}-C, whereas the second sample contained O9a polysaccharide without protein. Saturation times were tested at 1, 2, 3, and 6 s (Fig. 5*A*). It was determined that 3 s was sufficient for magnetization transfer, and data were collected. The most intense signal from the obtained STDD spectrum (aside from a differencing artifact arising from the Tris buffer) was a doublet at δ_H 3.63 ppm with coupling constant $J = 11$ Hz (Fig. 5*B*), which precisely corresponds to the chemical shift of the methyl protons on the nonreducing terminal methylphosphate group from O9a O-PS (33). These findings offer clear and direct data for the interaction of the nonreducing terminal methyl group with Wzt^{O9a}-C and are entirely consistent with its requirement for Wzt^{O9a}-C-binding in LPS pulldown experiments as well as its requirement for display of the O9a polysaccharide on the cell surface.

Identification of a terminal methylphosphate moiety in the K. pneumoniae O7 O-PS

The data above reveal the importance of the methylphosphate group for substrate recognition and export but do not reveal whether the terminal modification is sufficient by itself for these processes. To address this question, we examined the ability of the O9a CBM to bind an O-PS possessing a terminal methylphosphate group but a different repeat-unit structure. This was provided by *K. pneumoniae* O7, whose detailed structure has not been reported previously. Examination of the *K. pneumoniae* O7 *wb** locus (Fig. S1) revealed features consis-

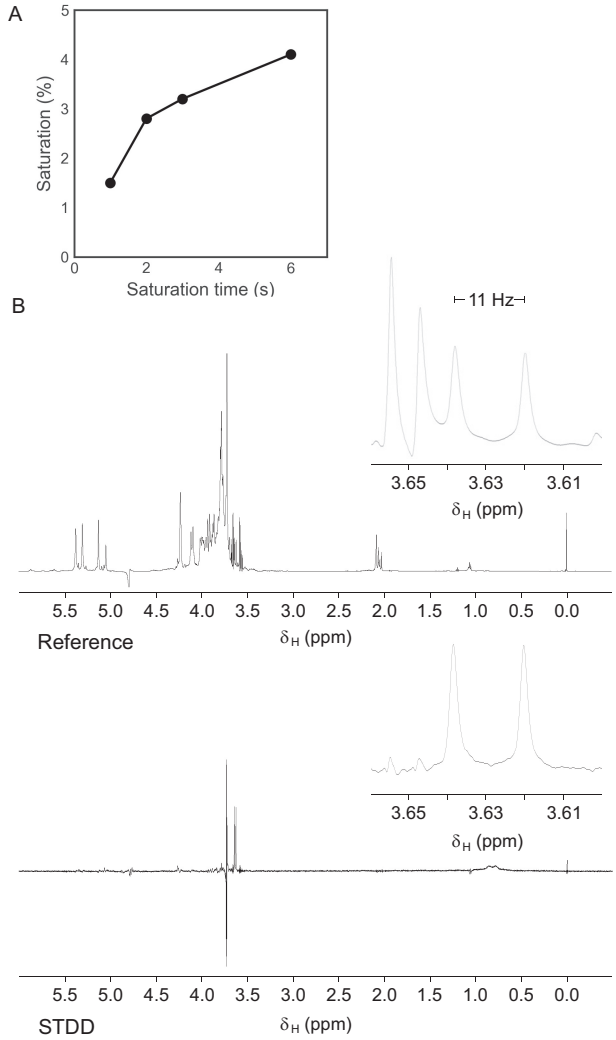

Figure 5. Wzt^{O9a}-C binds to the terminal methylphosphate group of the O9a polysaccharide. *A*, time dependence of magnetization transfer (*STDD*%) of the terminal methylphosphate methyl protons for four saturation time points. *B*, ^{1}H NMR spectra of off-resonance (*top*) and STDD (*bottom*) experiments after 3-s saturation. *Panels* to the *right* display the region between 3.60 and 3.66 ppm.

tent with chain-terminating ABC transporter-dependent O-PS biosynthesis. Wzt^{O7} possesses a proposed CBM domain sharing 34%/50% identity/similarity ($E = 7e^{-26}$) with the CBM of Wzt^{O9a} (Fig. 6*A*). A tertiary structure prediction of Wzt^{O7}-C using Phyre^{2} (34) indicates structural homology between the C-terminal domains (Fig. 6*B*). Furthermore, residues equivalent to those essential for Wzt^{O9a}-C O-PS binding, Trp-286, Gly-333, Asn-348, Gly-387, Arg-402, Tyr-404, and Asp-405 (23), are found in Wzt^{O7}-C. These similarities between the CBMs suggested that they recognize similar ligand structures, and therefore the O7 O-PS likely possesses a methylphosphate nonreducing terminal modification.

The O7 O-PS has a tetrasaccharide repeat unit [→2-α-L-Rha*p*-(1→2)-β-D-Rib*f*-(1→3)-α-L-Rha*p*-(1→3)-α-L-Rha*p*-(1→] (35). The previously reported structural study of O7 O-PS (32) was performed without the use of NMR spectroscopy and did not exclude the possibility that the anomeric configuration of one of the sugar residues could be reversed. Additionally, the possibility of terminal modification of O-PS chain was not investigated. We used ^{1}H, ^{13}C, and ^{31}P NMR spectroscopy, including two-dimensional ^{1}H,^{1}H correlation spectroscopy (COSY), total correlation spectroscopy (TOCSY), NOE spectroscopy (NOESY), heteronuclear single-quantum coherence (HSQC), heteronuclear multiple bond correlation (HMBC), and HMQC-TOCSY experiments to unequivocally determine the structure of the repeat unit and the nonreducing terminus of the O-PS. NMR spectra of O-PS contained the signals for four major spin systems, which were assigned to a Rib*f* residue (**A**) and three Rha*p* residues (**B**, **C**, and **D**) (Table 1, Fig. 7*A*, and Figs. S2–S4). The β-anomeric configuration of Rib was confirmed by the position of the Rib C-1 signal at δ 108.2 (compare published data (36) of δ 103.1 and 108.0 for methyl glycosides of α- and β-Rib*f*, respectively). The α-configuration of all three Rha residues were inferred from the H-5 and C-5 chemical shifts at δ_H 3.76–3.90 and δ_C 70.4–70.7 (compare published data (37) of δ_H 3.86, δ_C 69.1 for α-Rha*p*, δ_H 3.39, δ_C 72.8 for β-Rha*p*). These data, together with the sequence of the sugar residues determined by HMBC and NOESY (Fig. S2) experiments, confirmed the structure of O7 O-PS reported earlier (Fig. 7*A*).

In addition to the signals for sugar residues, the NMR spectra contained a characteristic sharp signal at δ_H/δ_C 3.63/54.3 with $J_{H,P}$ = 11 Hz, which was previously assigned to a methylphosphate group at the nonreducing terminus of *E. coli* O9a O-PS (33). The presence of a methylphosphate group was confirmed by correlation between methyl protons and phosphate at δ_H/δ_P 3.64/1.75 observed in the ^{1}H,^{31}P HMBC spectrum (Fig. 7*D*). Furthermore, a ^{1}H,^{31}P HMQC-TOCSY experiment showed correlation between phosphate and H-1 to H-5 of a minor α-Rha*p* spin system denoted as **B′.** The selective one-dimensional TOCSY (Fig. 7*B*) and NOESY experiments (not shown) confirmed the assignment of **B′** H-1 to H-6 signals. A relatively low-field position of the signal for **B′** C-3, together with strong HMBC correlation between phosphate and **B′** H-3, demonstrate that the methylphosphate group is attached at position O3 of **B′**. The linkage between **B′** and the next sugar residue could not be determined unambiguously, although the HMBC correlation at δ_H/δ_C 5.09/79.3 indicates that **B′** is linked to another Rha residue. Thus, the NMR spectroscopic analysis confirmed the structure of the O7 repeat unit reported earlier (35) and established the second known example of a methylphosphate O-PS terminal modification.

The methylphosphate group is necessary but not sufficient for CBM binding and transport

To examine whether the nonreducing terminal modification is the sole contributor to Wzt^{O9a}-C O-PS recognition, we performed a pulldown experiment using the *E. coli* O9a CBM with *K. pneumoniae* O7 LPS (Fig. 8, *A* and *B*). No O7 LPS was detected in elution fractions, indicating that the CBM did not bind O7 LPS. To validate these results, the reciprocal experiments were done using purified Wzt^{O7}-C. Evident from the silver stain, the O7 CBM was only able to bind its cognate LPS (Fig. 8, *C* and *D*). Finally, *in vivo* mutant complementation experiments were performed in *E. coli* O9a mutants lacking a functional O-PS ABC transporter (*manA* Δ*wzm-wzt*::*aphA-3*) (Fig. 9). Expression of the *K. pneumoniae* O7 ABC

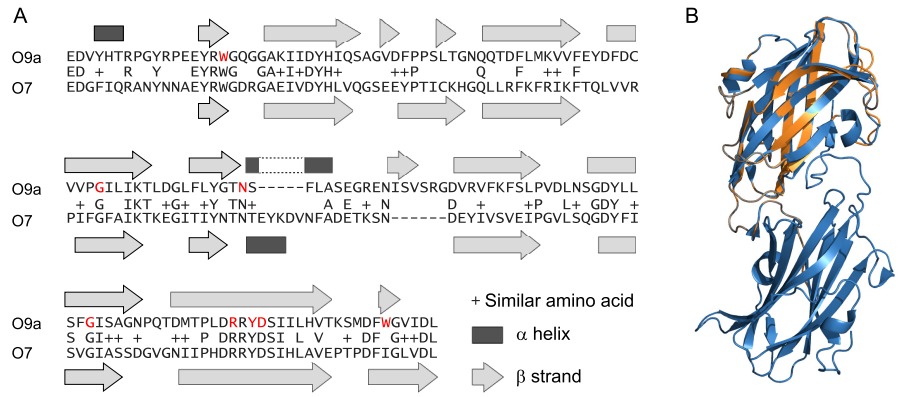

Figure 6. Alignment of Wzt^{O9a}-C (residues 270–423) to Wzt^{O7}-C (residues 303–455). *A*, pairwise sequence alignment was performed by Blast (*A*). The indicated secondary structure elements are from the Wzt^{O9a}-C crystal structure (Protein Data Bank entry 2R5O) and a Phyre^2 model of Wzt^{O7}-C. The residues coloured red are important for O-PS binding by Wzt^{O9a}-C (23). *B*, *cartoon representation overlay* of Wzt^{O7}-C model (*orange*) with Wzt^{O9a}-C crystal structure (*blue*). The structural overlay was generated using PyMOL (Schrödinger, LLC).

Table 1
^{1}H and ^{13}C NMR chemical shifts of *K. pneumoniae* 264(1) serotype O7 O-PS

Sugar residue	*H-1* C-1	*H-2* C-2	*H-3* C-3	*H-4* C-4	*H-5 (5a,b)* C-5	*H-6* C-6
Repeat unit						
→2)-*β*-D-Rib*f*-(1→						
A	*5.35*	*4.22*	*4.44*	*4.07*	*3.87, 3.71*	
	108.2	81.9	71.0	83.8	63.0	
→3)-*α*-D-Rha*p*-(1→						
B	*5.06*	*4.24*	*3.91*	*3.53*	*3.90*	*1.31*
	103.3	71.1	79.9	72.3	70.4	18.0
→3)-*α*-D-Rha*p*-(1→						
C	*4.98*	*4.18*	*3.85*	*3.57*	*3.80*	*1.29*
	103.2	71.1	79.4	72.5	70.7	17.9
→2)-*α*-D-Rha*p*-(1→						
D	*5.15*	*4.10*	*3.93*	*3.53*	*3.76*	*1.32*
	100.9	79.3	71.0	73.4	70.7	18.0
Non-reducing end[a]						
→3)-*α*-D-Rha*p*-(1→						
B′	*5.09*	*4.27*	*4.29*	*3.60*	*3.90*	*1.31*
	103.2	70.7	76.7	72.2	70.4	18.0

[a] The signals for the methylphosphate group are at δ_H 3.63, δ_C 54.3, and δ_P 1.75.

transporter in this mutant could not restore translocation of the O-PS across the inner membrane, as evidenced by the absence of banding on silver-stained SDS-polyacrylamide gels, consistent with results from *in vitro* pulldown experiments. Because the O7 and O9a LPS structures contain the same nonreducing terminal modification, the lack of O-PS binding and export must be due to differences in the main-chain polymer.

Discussion

The *E. coli* O9a O-PS biosynthesis and export system represents an elegant model for regulating polymer chain length distribution. By combining a molecular ruler with polymerization-termination and exporter-recognition mechanisms, the cell ensures an appropriate O-PS length distribution to optimize survival within the host. This system has become an important and influential prototype for similar strategies involved in the assembly of a variety of O-PS and other cell-surface glycans from Gram-negative and Gram-positive bacteria. The experimental platform for investigating substrate engagement by the *E. coli* O9a transporter therefore has broad relevance in microbial glycobiology.

Comparable systems have been identified in *E. coli* O8 and *K. pneumoniae* O12 and in S-layer glycoprotein assembly in *Geobacillus stearothermophilus* NRS2004/3a, *Geobacillus tepidamans* GS5-97^T, and *Aneurinibacillus thermoaerophilus* L420-91^T (27). In most examples, a single terminal residue (and presumed termination-export signal) is used. Examples include an *O*-methyl group on *E. coli* O8 O-PS and on the S-layer glycans from *G. stearothermophilus* NRS2004/3a (38) and *A. thermophilus* L420-91^T (39), as well as a Kdo on *K. pneumoniae* O12 (25). An exception is the addition of GlcNAc and *N*-acetylmuramic acid residues onto separate positions of the final rhamnose in *G. tepidimans* GS5-97^T (40), but only one of these residues is positioned to directly impede chain extension. The overall strategy for the biosynthesis of the terminally methylated D-rhamnose polymer in *G. stearothermophilus* NRS2004/3a is remarkably similar to that used for the methylated D-mannose *E. coli* O8 antigen (41). In contrast, *E. coli* O9a utilizes a binary terminator, consisting of a phosphate and an *O*-methyl group (18, 25). An identical structure terminates the related mannans produced by *E. coli* O9, *K. pneumoniae* O3a/O3b/O3c (42), and *Hafnia alvei* PCM1223 (33). This reflects lateral gene transfer of the locus, followed by diversification of the repeat-unit structure by mutations in *wbdA*. *K. pneumoniae* O7 uses the same methylphosphate terminating moiety to cap a different repeat-unit structure.

Despite the similar termination chemistry, the *K. pneumoniae* O7-biosynthesis gene cluster does not encode a homolog of the *E. coli* O9a WbdD protein. Instead, a candidate methyltransferase domain is part of a large multidomain predicted protein (Orf6) that also contains two candidate glycosyltransferases (belonging to family GT2) and a coiled-coil region (Fig. S1). This multidomain format is reminiscent of the *K. pneumoniae* O12 WbbB protein, where the terminating CMP-Kdo–dependent glycosyltransferase is separated by a coiled-coil domain from the glycosyltransferase modules that polymerize the repeat-unit glycan (43, 44). The kinase involved in the O7 termination reaction has not been identified, but, by analogy to WbdD, we anticipate this domain being located in proximity to the methyltransferase. Orf6 does possess an extensive region (47 kDa) downstream of the methyltransferase that could not be assigned by a homology search, and this may provide kinase activity. Because the identity of the kinase is not central to this

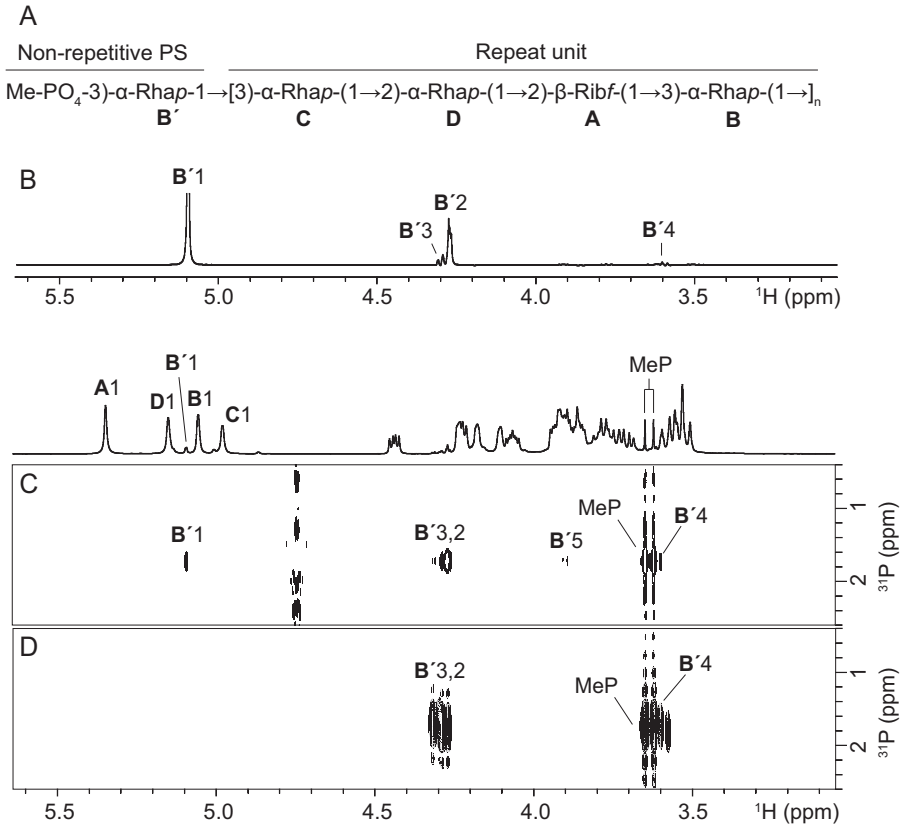

Figure 7. *K. pneumoniae* O7 O-PS is terminated with a methylphosphate group on C3 of the nonreducing terminal rhamnose residue. *A*, the determined repeat unit and nonreducing terminal structure of the O7 O-PS. Rha, L-rhamnose; Rib, D-ribose. *B*, part of the one-dimensional selective TOCSY spectrum obtained after irradiation of **B′** H-1 at δ 5.09. $^{1}H,^{31}P$ HMQC-TOCSY (*C*) and $^{1}H,^{31}P$ HMBC (*D*) spectra demonstrate correlations between phosphate and methyl protons as well as protons within the **B′** spin system. MeP, methylphosphate. The corresponding part of the ^{1}H NMR spectrum is shown along the *horizontal axis*.

study and is not required for data interpretation, it was not pursued here.

We demonstrated that the WbdD kinase domain was sufficient for chain length determination. However, the quality control mechanism conferred by the CBM shows an additional dependence on methyltransferase activity. STDD NMR experiments demonstrated that Wzt^{O9a}-C interacts directly with the methyl substituent at the nonreducing terminus, and this likely provides the most prominent hydrophobic interaction involved in O9a polysaccharide recognition by Wzt. The O9a CBM crystal structure has been solved, and the binding pocket was characterized using site-directed mutagenesis in conjugation with transport and CBM binding experiments (23). Several residues were necessary for substrate binding. Aromatic residues (Trp-286 and Tyr-404) presumably contribute via π-stacking with the monosaccharide rings, whereas polar residues (Asn-348, Arg-402, and Asp-405) may interact with sugar hydroxyl moieties or the terminal unit. Because these are conserved between Wzt^{O9a} and Wzt^{O7}, additional side chains distinct to each homologue must provide the noncovalent interactions critical for serotype specificity. However, these are not sufficient for robust productive binding in the absence of any terminal modification, as seen here and in previous experiments using *in vitro*–synthesized O9a glycan with or without complete terminal modification (23). STDD NMR experiments implicated the terminal methyl group as an interaction group with the CBM. Unfortunately, these experiments could not identify additional hydrophobic interactions arising from the main polymer, due to inefficient magnetization transfer. Furthermore, STD approaches are not suitable for identification of electrostatic or polar interactions. Interactions contributed by the main-chain polymer may be predominantly polar, arising from hydroxyl groups, and these are not detected because of the fast exchange of hydroxyl protons with solvent. It is likely that the phosphate moiety on the O9a glycan provides contact points within the binding pocket (*e.g.* through electrostatic interaction with the critical Arg-402 residue) (23) and therefore still contributes to recognition of the fully modified glycan. The extensive binding pocket likely accommodates main-chain sugars that contribute to the binding interface.

The O9a and O7 O-PS structures contain identical termination groups on the C-3 position of the nonreducing terminal sugar of their given polysaccharides. Because Wzt^{O9a}-C did not interact with O7 LPS during pulldown experiments, we conclude that one or more monosaccharide units provide functional groups that contribute to direct interactions with the CBM. Cocrystal structures with terminated O-PS analogues are essential to conclusively verify structural features related to O-PS specificity, but, to date, we have been unable to obtain structures of CBM:O-PS complexes for a detailed view of the interactions.

Here, we focus solely on the role of the terminal modification in the substrate recognition process. How this interfaces with substrate engagement by the transporter proper remains to be

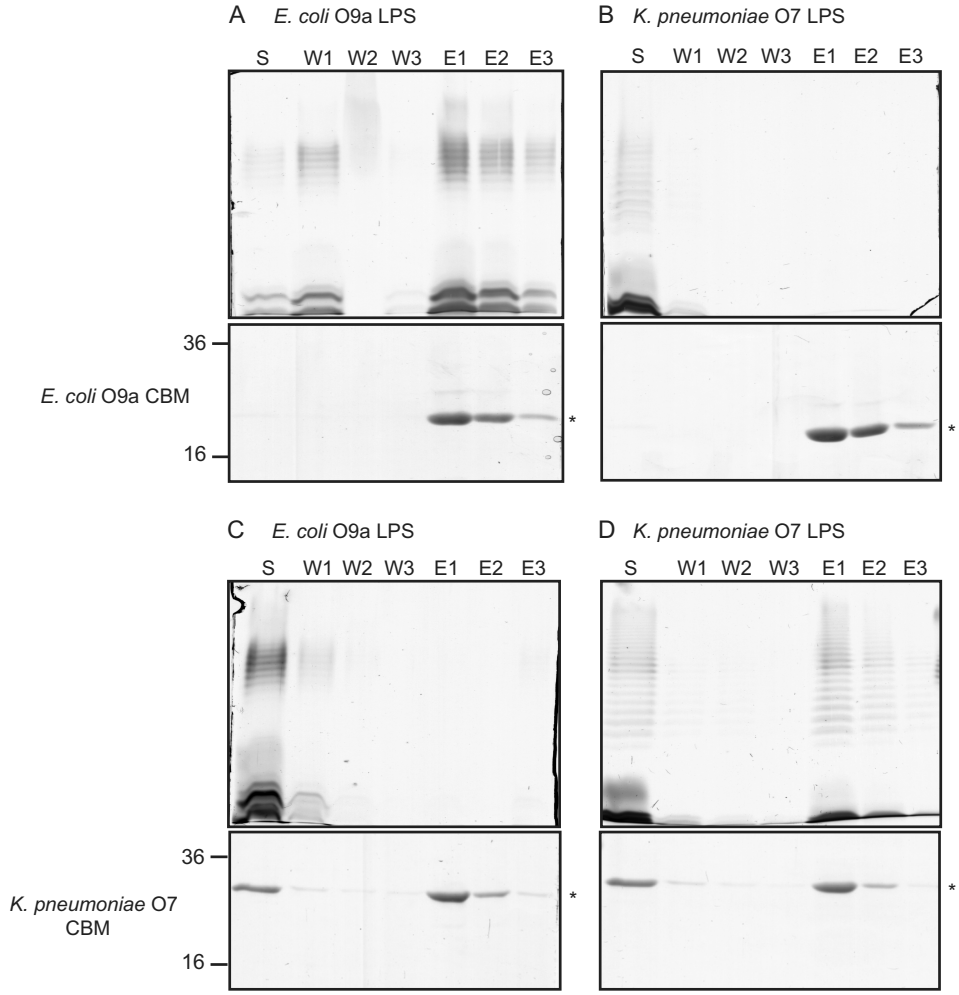

Figure 8. Wzt^{O9a}-C and Wzt^{O7}-C can only bind LPS from the native serotype. Purified Wzt^{O9a}-C (O9a CBM; *A* and *B*) and Wzt^{O7}-C (O7 CBM; *C* and *D*) were incubated with the O9a and O7 LPSs. Reaction mixtures consisting of 200 μg of CBM and 200 μg of LPS were mixed with nickel magnetic beads and collected using a magnet. The samples are unbound material in the supernatant (*S*) and material released by sequential washes of the beads in the absence (*W1–W3*) or presence of imidazole (*E1–E3*). Aliquots of the collected samples were subjected to SDS-PAGE. LPS was detected by silver staining (*top panels*), and protein was detected by simply blue staining (*bottom panels*).

resolved. The ultimate goal of this and related studies is to recapitulate the export process with purified proteins and substrates in proteoliposomes, and, in this context, resolution of the chemical determinants for export is a critical step toward this objective. However, why *E. coli* O9a has evolved and maintained a more complex strategy, compared with the simple methylation process in the related *E. coli* O8, remains unanswered.

Experimental procedures

Strains, plasmids, and growth conditions

The bacterial strains and plasmids used in this study are described in Table 2. Cultures were grown in lysogeny broth (LB) at 37 °C with aeration and were supplemented with 100 μg ml^{-1} of ampicillin, D-glucose (0.4% w/v), D-mannose (0.4% w/v), or L-arabinose (0.0002–0.2% (w/v)) where appropriate, unless otherwise specified.

DNA methods

KOD Hot Start DNA polymerase (Novagen) was used for cloning DNA fragments. Oligonucleotide primers were obtained from Sigma and are listed in Table S1. Amplified products were purified using a GeneJET purification kit (Thermo Fisher Scientific), and restriction endonuclease digests were performed using enzymes from New England Biolabs. Restriction sites used are indicated in Table 1. Plasmids were confirmed by restriction digests and by DNA sequencing performed by the Advanced Analysis Centre, University of Guelph.

Construction of E. coli CWG1412

E. coli CWG1412 (*manA wbdD*::aacC1 Δ*wzm-wzt*::*aphA-3*) was constructed using the same primers and protocol as described previously for construction of CWG638 (17). However, CWG635 was used as the parent strain instead of CWG634.

Genomic DNA sequencing

Whole-genome shotgun sequence data for *K. pneumoniae* 264(1) was generated using the Solexa paired-end sequencing platform (Illumina) and genomic DNA prepared using the Illumina sample preparation kit. *De novo* assembly of sequencing reads (~100× coverage) was performed with Velvet (45). The

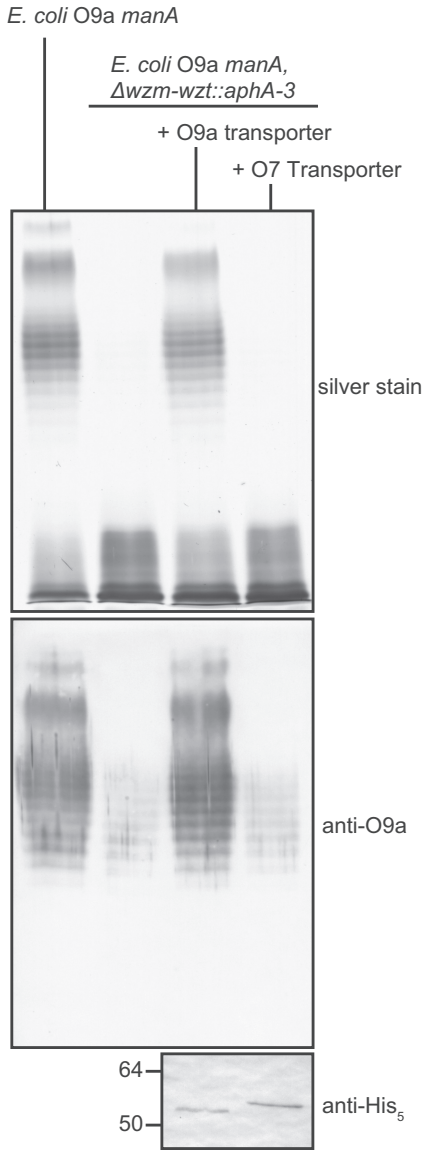

Figure 9. The *K. pneumoniae* O7 ABC transporter is unable to export the *E. coli* O9a O-PS. Overnight cultures of *E. coli manA* (CWG634; O9a O-PS control) *and E. coli manA* Δ*wzm-wzt::aph3-A* (CWG638) transformed with plasmids encoding either the O9a (pWQ332) or O7 (pWQ1014) transporter (Wzm-Wzt-His_6) were subcultured for 3 h in medium supplemented with 0.1% D-mannose and 0.1% L-arabinose to induce O-PS biosynthesis and transporter expression, respectively. LPS profiles were examined in proteinase K–treated whole-cell lysates using silver-stained SDS-polyacrylamide gels (*top*). α-His_5 Western blots of whole cell lysates were used to confirm transporter expression (*bottom*). O-PS present in *lanes 2* and *4* of the Western blot is a result of nonexported O-PS, evident from its lack of silver staining.

sequence of the gene cluster for O7 O-PS biosynthesis has been deposited in NCBI (GenBank™ accession no. MN173773).

SDS-PAGE and immunoblotting

To prepare whole-cell lysates for SDS-PAGE and Western immunoblotting, bacterial cells (1 $A_{600\ nm}$ unit equivalent) were collected by centrifugation, solubilized in SDS-PAGE loading buffer, and heated to 100 °C for 10 min prior to electrophoresis. For LPS analysis, the whole-cell lysates were treated with proteinase K (Invitrogen) for 1 h at 55 °C (46). SDS-PAGE was performed using 12% acrylamide resolving gels in Tris-glycine buffer (47). LPS was visualized by staining with a silver nitrate solution (48), and protein was detected using SimplyBlue SafeStain (Invitrogen).

For immunoblot analyses, material resolved by SDS-PAGE was transferred to nitrocellulose membranes (Protran; PerkinElmer Life Sciences). O9a antigen was detected using polyclonal antibodies raised in rabbits (17). Alkaline phosphatase–conjugated goat anti-rabbit was used as a secondary antibody (Cedar Lane Laboratories). Hexahistidine-tagged proteins were detected using mouse-anti-His_5 mAb (Qiagen) and alkaline phosphatase-conjugated goat anti-mouse secondary antibody (CedarLane Laboratories). Immunoblots were developed with nitro blue tetrazolium and 5-bromo-4-chloro-3-indoyl phosphate (Roche Applied Science).

Immunofluorescence microscopy

Overnight cultures grown in LB, 0.4% D-glucose were subcultured 1:100 into fresh LB, glucose. After 4 h, cells were resuspended in fresh medium containing 0.4% D-mannose and 0.02% L-arabinose to facilitate WbdD synthesis, and growth was continued for an additional 1 h before cells were harvested. Microscopy was performed on formaldehyde-fixed whole cells as described previously (17), using rabbit-anti-O9a primary antibody and FITC-conjugated goat anti-rabbit secondary antibody (Thermo Fisher Scientific).

Wzt-C purification

Wzt^{O9a}-C was purified as described previously (23). Briefly, *E. coli* Top10 harboring pWQ424 was grown at 37 °C with aeration to mid-exponential growth phase and induced with 0.3% L-arabinose for an additional 2 h. Cells were collected by centrifugation, resuspended in buffer A (25 mM Tris, pH 7.5, containing 100 mM NaCl), and lysed by sonication. Cleared lysate was applied to 1-ml columns of nickel affinity resin. Resin was washed with buffer A containing 20 mM imidazole, and protein was eluted using buffer A containing 200 mM imidazole. Wzt^{O7}-C was purified from *E. coli* Top10 harboring pWQ1013, using the same growth and induction conditions. Wzt^{O7}-C was also purified by nickel-affinity chromatography, but buffer B (25 mM Bis-Tris, pH 7.0, 250 mM NaCl) was used.

LPS purification

WT *E. coli* O9a LPS was purified from overnight cultures of *E. coli* CWG28 and E69 for pulldown experiments and STDD NMR experiments, respectively. WT *K. pneumoniae* O7 LPS was purified from *K. pneumoniae* 264(1). LPS containing non-terminated O-PS was prepared from *E. coli* CWG1412 (*manA wbdD::aacC1* Δ*wzm-wzt::aphA-3*), which lacks innate termination and transport activities, transformed with pWQ391, which provides the ABC transporter from *K. pneumoniae* O2a. This transporter operates independently of O-PS repeat-unit structure and does not require a terminating moiety (11, 12). LPS lacking a nonreducing terminal O-PS modification was purified from *E. coli* CWG1412 transformed with pWQ391 and either pWQ830 ($WbdD^{D351A}$) or pWQ831 (*wbdD*^{Y16F}). The $WbdD^{Y16F}$ variant lacks methyltransferase activity (19). L-Arabinose (0.1%) was added to induce the recombinant *K. pneumoniae* O2a ABC transporter. After 30 min of growth, D-man-

Table 2
List of strains and plasmids

Strain/plasmid name	Description	Source
Strain		
E. coli E69	Serotype O9a:K30	F. Orskov
K. pneumoniae 264(1)	Serotype O7:K67	F. Orskov
CWG28	*E. coli* E69 derivative; *trp his lac rpsL* cps_{K30}; Sm^r	Ref. 52
CWG634	CWG28 derivative; *manA*; Sm^r, Tc^r	Ref. 17
CWG635	CWG634 derivative; *wbdD*::aacC1; Sm^r, Tc^r, Gm^r	Ref. 17
CWG638	CWG634 derivative; Δ*wzm-wzt*::*aphA-3*; Sm^r Tc^r Km^r	Ref. 17
CWG900	CWG634 derivative; Δ*wbdD*; Sm^r, Tc^r	Ref. 16
CWG1412	CWG635 derivative; Δ*wzm-wzt*::*aphA-3*; Sm^r Tc^r Km^r, Gm^r	This study
Plasmid		
pBAD24	Plasmid vector with L-arabinose-inducible promoter; Ap^r	Ref. 53
pKD3	Source of chloramphenicol resistance cassette; Cm^r	Ref. 54
pWQ470	pBAD24 derivative containing His_6-*wbdD*	Ref. 16
pWQ829	pWQ470 derivative containing His_6-$wbdD^{H132A}$	Ref. 19
pWQ830	pWQ470 derivative containing His_6-$wbdD^{D351A}$	Ref. 19
pWQ831	pWQ470 derivative containing His_6-$wbdD^{Y16FA}$	Ref. 19
pWQ391	pBAD24 derivative containing a fragment including *wzm-wzt* from *K. pneumoniae* O2a and the Cm^r cassette from pKD3 cloned into the ScaI site; Cm^r	Ref. 11
pWQ1013	pBAD24 derivative containing the open-reading frame encoding His_6-Wzt-C (amino acids 268–464) from *K. pneumoniae* O7 cloned between the NheI and NcoI sites	This study
pWQ1014	pBAD24 derivative containing the open reading frame encoding Wzm-Wzt-His_6 tag from *K. pneumoniae* O7 cloned between the NheI and NcoI sites	This study
pWQ332	pBAD24 derivative containing *E. coli* O9a Wzm-Wzt-His_6	Ref. 22
pWQ424	pBAD24 derivative containing *E. coli* O9a Wzt-C-His_{10}	Ref. 23

nose (0.4%) was added to initiate O-PS expression, and the cultures were grown for an additional 2 h. LPS was purified using the hot water phenol method (49). After dialysis of the extraction mixture against water to remove the phenol, proteins and nucleic acids were precipitated using cold, aqueous TCA and dialyzed until neutral. To separate O7 LPS from capsule, LPS was sedimented by ultracentrifugation for 18 h at 100,000 × *g* in 20 mM NaOAc, pH 7.0.

O-PS for NMR analysis was isolated by acid hydrolysis of LPS at 100 °C in 2% (v/v) acetic acid, followed by centrifugation at 13,000 × *g* to remove lipid precipitate. The carbohydrate-containing supernatant was fractionated on a Sephadex G-50 superfine column (2.5 × 75 cm) in 50 mM pyridinium acetate buffer (pH 4.5) at a flow rate of 0.6 ml min^{-1}. Elution was monitored with a Smartline 2300 refractive index detector (Knauer). The O9a O-PS–containing fraction was acidic (potentially due to contaminating capsule; data not shown), so the polysaccharide mixture was applied to a DEAE Fast Flow (GE Healthcare) column and eluted with a 5–500 mM sodium phosphate gradient at pH 6.3 monitored using absorbance spectroscopy at a wavelength of 208 nm (50). The O9a polysaccharide-containing fractions were pooled and buffer-exchanged by chromatography on a Sephadex G-50 superfine column equilibrated with water.

Binding assays

In vitro binding assays were performed as described previously (12, 23). 1-ml reaction volumes of buffer B (25 mM Bis-Tris, pH 7.0, 250 mM NaCl) containing 200 μg of LPS and 200 μg of Wzt-C were incubated on a rotary shaker for 30 min at room temperature. This mixture was added to 50 μl of PureProteome nickel magnetic beads (Millipore), which were pre-equilibrated with buffer B, and incubated for 30 min at room temperature on a rotary shaker. The beads were collected with a magnet and washed three times with 500 μl of buffer B. Protein was eluted stepwise from the beads using three washes with 100 μl of buffer B containing 500 mM imidazole.

STDD NMR

NMR studies were performed at the University of Guelph Advanced Analysis Centre. The chemical shifts are referenced to 3-trimethylsilylpropanoate-2,2,3,3-d_4 (δ_H 0, δ_C −1.6) added as an internal standard. The Bruker TopSpin 3.2 program was used to acquire and process the NMR data.

STD NMR samples contained 22.2 mg/ml (estimated 2.2 mM) O9a polysaccharide and 0.022 mM Wzt^{O9a}-C (omitted for the "double difference" sample) in 25 mM Tris, pH 7.4, 100 mM NaCl. Deuterium oxide was added to 10% (v/v). NMR spectra were collected on a Bruker AVANCE III 600-MHz spectrometer equipped with a 5-mm TCI cryoprobe. The sample temperature was regulated at 298.2 ± 1 K. STD spectra (28) were acquired using the Bruker pulse sequence *stddiffesgp*, which suppresses the water resonance via an excitation sculpting scheme (51). Wzt^{O9a}-C was saturated with a train of Gaussian-shaped pulses of 25 ms each (calibrated to the correct power level for a 90° Gaussian pulse), applied at 0.67 ppm for the "on-resonance" spectrum and at −11.66 ppm for the "off-resonance" spectrum. Four different irradiation times of 1, 2, 3, and 6 s were employed, and the total prescan delay (*i.e.* including the irradiation time) was kept constant at 7 s. The acquisition time was 1.7 s. STD data were obtained by subtracting the on-resonance FID from the off-resonance FID using the *stdsplit* macro provided by the Bruker software program TopSpin.

The frequency-selective pulse employed in the excitation sculpting scheme is not infinitely narrow and can cause undesired attenuation of nearby ligand resonances (*e.g.* anomeric protons). In the default implementation, the frequency-selective pulse duration is 2 ms, which resulted in the undesired suppression of the anomeric proton resonance at 5.04 ppm to 6% of its nominal intensity. For the experiments presented in this paper, the frequency-selective pulse duration was increased to 5 ms; the reduction in the corresponding pulse bandwidth restored the intensity of the 5.04-ppm anomeric proton to 80% of the nominal value.

When performed on larger ligands, the STD experiment can result in partial saturation of the ligand. To correct for this, a set of "ligand-only" STD experiments were performed on a second sample not containing Wzt^{O9a}-C (but otherwise identical to the sample described above), and the resulting "ligand-only" STD data were subtracted from the STD data of O9a in the presence of Wzt^{O9a}-C to produce the STDD spectra reported (32).

Elucidation of the K. pneumoniae O7 O-PS structure

O-PS samples were lyophilized twice in 99.9% D_2O for deuterium exchange and then analyzed in 99.9% D_2O at 30 °C. Data were collected using a Bruker Avance III 600-MHz spectrometer equipped with a 5-mm TCI cryoprobe, with the exception of ^{31}P-based NMR experiments, performed on a Bruker 400-MHz Avance III spectrometer equipped with a 5-mm broadband Prodigy cryoprobe. Mixing times of 100 and 200 ms were used in TOCSY and NOESY experiments, respectively. The HMBC experiment was optimized for the $J_{H,C}$ coupling constant of 8 Hz and a $J_{H,P}$ coupling constant of 11 Hz. Mixing times of 100 and 80 ms were used for selective TOCSY and $^{1}H,^{31}P$ HMQC-TOCSY, respectively.

Author contributions—E. M., S. D. K., and C. W. conceived the study. E. M., S. D. K., and S. A. performed the experiments. B. L. provided genome sequence data. E. M., S. D. K., S. A., B. R. C., O. G. O., and C. W. analyzed and interpreted the data. E. M., S. D. K., S. A., O. G. O., and C. W. prepared the initial manuscript draft, and all authors provided input for the final version.

Acknowledgments—We are grateful to Dr. Vladimir Ladizhansky for helpful discussions concerning NMR experiments, Gregory Whitfield for purifying Wzt^{O9a}-C and LPS, and Lu Wang and Xi Gou for genomic sequence data.

References

1. Whitfield, C., and Trent, M. S. (2014) Biosynthesis and export of bacterial lipopolysaccharides. *Annu. Rev. Biochem.* **83,** 99–128 CrossRef Medline
2. Raetz, C. R. H., and Whitfield, C. (2002) Lipopolysaccharide endotoxins. *Annu. Rev. Biochem.* **71,** 635–700 CrossRef Medline
3. Lerouge, I., and Vanderleyden, J. (2002) O-antigen structural variation: mechanisms and possible roles in animal/plant-microbe interactions. *FEMS Microbiol. Rev.* **26,** 17–47 CrossRef Medline
4. Grossman, N., Schmetz, M. A., Foulds, J., Klima, E. N., Jimenez-Lucho, V. E., Leive, L. L., Joiner, K. A., and Jiminez, V. (1987) Lipopolysaccharide size and distribution determine serum resistance in *Salmonella montevideo*. *J. Bacteriol.* **169,** 856–863 CrossRef Medline
5. Burns, S. M., and Hull, S. I. (1998) Comparison of loss of serum resistance by defined lipopolysaccharide mutants and an acapsular mutant of uropathogenic *Escherichia coli* O75:K5. *Infect. Immun.* **66,** 4244–4253 Medline
6. Mostowy, R. J., and Holt, K. E. (2018) Diversity-generating machines: genetics of bacterial sugar-coating. *Trends Microbiol.* **26,** 1008–1021 CrossRef Medline
7. Greenfield, L. K., and Whitfield, C. (2012) Synthesis of lipopolysaccharide O-antigens by ABC transporter-dependent pathways. *Carbohydr. Res.* **356,** 12–24 CrossRef Medline
8. Liston, S. D., Mann, E., and Whitfield, C. (2017) Glycolipid substrates for ABC transporters required for the assembly of bacterial cell-envelope and cell-surface glycoconjugates. *Biochim. Biophys. Acta Mol. Cell. Biol. Lipids* **1862,** 1394–1403 CrossRef Medline
9. Okuda, S., Sherman, D. J., Silhavy, T. J., Ruiz, N., and Kahne, D. (2016) Lipopolysaccharide transport and assembly at the outer membrane: the PEZ model. *Nat. Rev. Microbiol.* **14,** 337–345 CrossRef Medline
10. Sperandeo, P., Martorana, A. M., and Polissi, A. (2017) The lipopolysaccharide transport (Lpt) machinery: A nonconventional transporter for lipopolysaccharide assembly at the outer membrane of Gram-negative bacteria. *J. Biol. Chem.* **292,** 17981–17990 CrossRef Medline
11. Kos, V., Cuthbertson, L., and Whitfield, C. (2009) The *Klebsiella pneumoniae* O2a antigen defines a second mechanism for O antigen ATP-binding cassette transporters. *J. Biol. Chem.* **284,** 2947–2956 CrossRef Medline
12. Mann, E., Mallette, E., Clarke, B. R., Kimber, M. S., and Whitfield, C. (2016) The *Klebsiella pneumoniae* O12 ATP-binding Cassette (ABC) transporter recognizes the terminal residue of its O-antigen polysaccharide substrate. *J. Biol. Chem.* **291,** 9748–9761 CrossRef Medline
13. Greenfield, L. K., Richards, M. R., Li, J., Wakarchuk, W. W., Lowary, T. L., and Whitfield, C. (2012) Biosynthesis of the polymannose lipopolysaccharide O-antigens from *Escherichia coli* serotypes O8 and O9a requires a unique combination of single- and multiple-active site mannosyltransferases. *J. Biol. Chem.* **287,** 35078–35091 CrossRef Medline
14. Liston, S. D., Clarke, B. R., Greenfield, L. K., Richards, M. R., Lowary, T. L., and Whitfield, C. (2015) Domain interactions control complex formation and polymerase specificity in the biosynthesis of the *Escherichia coli* O9a antigen. *J. Biol. Chem.* **290,** 1075–1085 CrossRef Medline
15. Greenfield, L. K., Richards, M. R., Vinogradov, E., Wakarchuk, W. W., Lowary, T. L., and Whitfield, C. (2012) Domain organization of the polymerizing mannosyltransferases involved in synthesis of the *Escherichia coli* O8 and O9a lipopolysaccharide O-antigens. *J. Biol. Chem.* **287,** 38135–38149 CrossRef Medline
16. Clarke, B. R., Greenfield, L. K., Bouwman, C., and Whitfield, C. (2009) Coordination of polymerization, chain termination, and export in assembly of the *Escherichia coli* lipopolysaccharide O9a antigen in an ATP-binding cassette transporter-dependent pathway. *J. Biol. Chem.* **284,** 30662–30672 CrossRef Medline
17. Clarke, B. R., Cuthbertson, L., and Whitfield, C. (2004) Nonreducing terminal modifications determine the chain length of polymannose O antigens of *Escherichia coli* and couple chain termination to polymer export via an ATP-binding cassette transporter. *J. Biol. Chem.* **279,** 35709–35718 CrossRef Medline
18. Clarke, B. R., Richards, M. R., Greenfield, L. K., Hou, D., Lowary, T. L., and Whitfield, C. (2011) *In vitro* reconstruction of the chain termination reaction in biosynthesis of the *Escherichia coli* O9a O-polysaccharide: the chain-length regulator, WbdD, catalyzes the addition of methyl phosphate to the non-reducing terminus of the growing glycan. *J. Biol. Chem.* **286,** 41391–41401 CrossRef Medline
19. Hagelueken, G., Huang, H., Clarke, B. R., Lebl, T., Whitfield, C., and Naismith, J. H. (2012) Structure of WbdD: a bifunctional kinase and methyltransferase that regulates the chain length of the O antigen in *Escherichia coli* O9a. *Mol. Microbiol.* **86,** 730–742 CrossRef Medline
20. Hagelueken, G., Clarke, B. R., Huang, H., Tuukkanen, A., Danciu, I., Svergun, D. I., Hussain, R., Liu, H., Whitfield, C., and Naismith, J. H. (2015) A coiled-coil domain acts as a molecular ruler to regulate O-antigen chain length in lipopolysaccharide. *Nat. Struct. Mol. Biol.* **22,** 50–56 CrossRef Medline
21. King, J. D., Berry, S., Clarke, B. R., Morris, R. J., and Whitfield, C. (2014) Lipopolysaccharide O antigen size distribution is determined by a chain extension complex of variable stoichiometry in *Escherichia coli* O9a. *Proc. Natl. Acad. Sci. U.S.A.* **111,** 6407–6412 CrossRef Medline
22. Cuthbertson, L., Powers, J., and Whitfield, C. (2005) The C-terminal domain of the nucleotide-binding domain protein Wzt determines substrate specificity in the ATP-binding cassette transporter for the lipopolysaccharide O-antigens in *Escherichia coli* serotypes O8 and O9a. *J. Biol. Chem.* **280,** 30310–30319 CrossRef Medline
23. Cuthbertson, L., Kimber, M. S., and Whitfield, C. (2007) Substrate binding by a bacterial ABC transporter involved in polysaccharide export. *Proc. Natl. Acad. Sci. U.S.A.* **104,** 19529–19534 CrossRef Medline
24. Bi, Y., Mann, E., Whitfield, C., and Zimmer, J. (2018) Architecture of a channel-forming O-antigen polysaccharide ABC transporter. *Nature* **553,** 361–365 CrossRef Medline
25. Vinogradov, E., Frirdich, E., MacLean, L. L., Perry, M. B., Petersen, B. O., Duus JØ., Whitfield, C. (2002) Structures of lipopolysaccharides from

Klebsiella pneumoniae: eluicidation of the structure of the linkage region between core and polysaccharide O chain and identification of the residues at the non-reducing termini of the O chains. *J. Biol. Chem.* **277,** 25070–25081 CrossRef Medline

26. Mann, E., Ovchinnikova, O. G., King, J. D., and Whitfield, C. (2015) Bacteriophage-mediated glucosylation can modify lipopolysaccharide O-antigens synthesized by an ATP-binding cassette (ABC) transporter-dependent assembly mechanism. *J. Biol. Chem.* **290,** 25561–25570 CrossRef Medline
27. Cuthbertson, L., Kos, V., and Whitfield, C. (2010) ABC transporters involved in export of cell surface glycoconjugates. *Microbiol. Mol. Biol. Rev.* **74,** 341–362 CrossRef Medline
28. Mayer, M., and Meyer, B. (1999) Characterization of ligand binding by saturation transfer difference NMR spectroscopy. *Angew. Chem. Int. Ed. Engl.* **38,** 1784–1788 CrossRef Medline
29. van de Weerd, R., Berbís, M. A., Sparrius, M., Maaskant, J. J., Boot, M., Paauw, N. J., de Vries, N., Boon, L., Baba, O., Cañada, F. J., Geurtsen, J., Jiménez-Barbero, J., and Appelmelk, B. J. (2015) A murine monoclonal antibody to glycogen: characterization of epitope-fine specificity by saturation transfer difference (STD) NMR spectroscopy and its use in mycobacterial capsular α-glucan research. *Chembiochem* **16,** 977–989 CrossRef Medline
30. Kooistra, O., Herfurth, L., Lüneberg, E., Frosch, M., Peters, T., and Zähringer, U. (2002) Epitope mapping of the O-chain polysaccharide of *Legionella pneumophila* serogroup 1 lipopolysaccharide by saturation-transfer-difference NMR spectroscopy. *Eur. J. Biochem.* **269,** 573–582 CrossRef Medline
31. Mayer, M., and Meyer, B. (2001) Group epitope mapping by saturation transfer difference NMR to identify segments of a ligand in direct contact with a protein receptor. *J. Am. Chem. Soc.* **123,** 6108–6117 CrossRef Medline
32. Claasen, B., Axmann, M., Meinecke, R., and Meyer, B. (2005) Direct observation of ligand binding to membrane proteins in living cells by a saturation transfer double difference (STDD) NMR spectroscopy method shows a significantly higher affinity of integrin $\alpha_{IIb}\beta_3$ in native platelets than in liposomes. *J. Am. Chem. Soc.* **127,** 916–919 CrossRef Medline
33. Kubler-Kielb, J., Whitfield, C., Katzenellenbogen, E., and Vinogradov, E. (2012) Identification of the methyl phosphate substituent at the non-reducing terminal mannose residue of the O-specific polysaccharides of *Klebsiella pneumoniae O3*, *Hafnia alvei* PCM 1223 and *Escherichia coli* O9/O9a LPS. *Carbohydr. Res.* **347,** 186–188 CrossRef Medline
34. Kelley, L. A., Mezulis, S., Yates, C. M., Wass, M. N., and Sternberg, M. J. E. (2015) The Phyre2 web portal for protein modeling, prediction and analysis. *Nat. Protoc.* **10,** 845–858 CrossRef Medline
35. Lindberg, B., Lönngren, J., Nimmich, W., and Rudén, U. (1973) Structural studies on the *Klebsiella* O group 7 lipopolysaccharide. *Acta Chem. Scand.* **27,** 3787–3790 CrossRef Medline
36. Bock, K., and Pedersen, C. (1983) Carbon-13 nuclear magnetic resonance spectroscopy of monosaccharides. *Adv. Carbohydr. Chem. Biochem.* **41,** 27–66 CrossRef
37. Jansson, P. E., Kenne, L., and Widmalm, G. (1989) Computer-assisted structural analysis of polysaccharides with an extended version of casper using ^{1}H- and ^{13}C-N.M.R. data. *Carbohydr. Res.* **188,** 169–191 CrossRef Medline
38. Schäffer, C., Wugeditsch, T., Kählig, H., Scheberl, A., Zayni, S., and Messner, P. (2002) The surface layer (S-layer) glycoprotein of *Geobacillus stearothermophilus* NRS 2004/3a: analysis of its glycosylation. *J. Biol. Chem.* **277,** 6230–6239 CrossRef Medline
39. Schäffer, C., Müller, N., Christian, R., Graninger, M., Wugeditsch, T., Scheberl, A., and Messner, P. (1999) Complete glycan structure of the S-layer glycoprotein of *Aneurinibacillus thermoaerophilus* GS4–GS97. *Glycobiology* **9,** 407–414 CrossRef Medline
40. Kählig, H., Kolarich, D., Zayni, S., Scheberl, A., Kosma, P., Schäffer, C., and Messner, P. (2005) *N*-acetylmuramic acid as capping element of α-D-fucose-containing S-layer glycoprotein glycans from *Geobacillus tepidamans* GS5–97T. *J. Biol. Chem.* **280,** 20292–20299 CrossRef Medline
41. Steiner, K., Novotny, R., Werz, D. B., Zarschler, K., Seeberger, P. H., Hofinger, A., Kosma, P., Schäffer, C., and Messner, P. (2008) Molecular basis of S-layer glycoprotein glycan biosynthesis in *Geobacillus stearothermophilus*. *J. Biol. Chem.* **283,** 21120–21133 CrossRef Medline
42. Guachalla, L. M., Stojkovic, K., Hartl, K., Kaszowska, M., Kumar, Y., Wahl, B., Paprotka, T., Nagy, E., Lukasiewicz, J., Nagy, G., and Szijártó, V. (2017) Discovery of monoclonal antibodies cross-reactive to novel subserotypes of *K. pneumoniae* O3. *Sci. Rep.* **7,** 6635 CrossRef Medline
43. Williams, D. M., Ovchinnikova, O. G., Koizumi, A., Mainprize, I. L., Kimber, M. S., Lowary, T. L., and Whitfield, C. (2017) Single polysaccharide assembly protein that integrates polymerization, termination, and chain-length quality control. *Proc. Natl. Acad. Sci. U.S.A.* **114,** E1215–E1223 CrossRef Medline
44. Ovchinnikova, O. G., Mallette, E., Koizumi, A., Lowary, T. L., Kimber, M. S., and Whitfield, C. (2016) Bacterial β-Kdo glycosyltransferases represent a new glycosyltransferase family (GT99). *Proc. Natl. Acad. Sci. U.S.A.* **113,** E3120–E3129 CrossRef Medline
45. Zerbino, D. R., and Birney, E. (2008) Velvet: algorithms for *de novo* short read assembly using de Bruijn graphs. *Genome Res.* **18,** 821–829 CrossRef Medline
46. Hitchcock, P. J., and Brown, T. M. (1983) Morphological heterogeneity among *Salmonella* lipopolysaccharide chemotypes in silver-stained polyacrylamide gels. *J. Bacteriol.* **154,** 269–277 Medline
47. Laemmli, U. K. (1970) Cleavage of structural proteins during the assembly of the head of bacteriophage T4. *Nature* **227,** 680–685 CrossRef Medline
48. Tsai, C. M., and Frasch, C. E. (1982) A sensitive silver stain for detecting lipopolysaccharides in polyacrylamide gels. *Anal. Biochem.* **119,** 115–119 CrossRef Medline
49. Westphal, O. (1965) Bacterial lipopolysaccharide-extraction with phenol water and further application of procedure. *Methods Carbohydr. Chem.* **1,** 83–91
50. Fedonenko, Y. P., Zatonsky, G. V., Konnova, S. A., Zdorovenko, E. L., and Ignatov, V. V. (2002) Structure of the O-specific polysaccharide of the lipopolysaccharide of *Azospirillum brasilense* Sp245. *Carbohydr. Res.* **337,** 869–872 CrossRef Medline
51. Hwang, T. L., and Shaka, A. J. (1995) Water suppression that works: excitation sculpting using arbitrary waveforms and pulsed field gradients. *J. Magn. Reson. Ser. A* **112,** 275–279 CrossRef
52. Whitfield, C., Schoenhals, G., and Graham, L. (1989) Mutants of *Escherichia coli* O9:K30 with altered synthesis and expression of the capsular K30 antigen. *J Gen Microbiol.* **135,** 2589–2599 Medline
53. Guzman, L. M., Belin, D., Carson, M. J., and Beckwith, J. (1995) Tight regulation, modulation, and high-level expression by vectors containing the arabinose PBAD promoter. *J. Bacteriol.* **177,** 4121–4130 CrossRef Medline
54. Datsenko, K. A., and Wanner, B. L. (2000) One-step inactivation of chromosomal genes in *Escherichia coli* K-12 using PCR products. *Proc. Natl. Acad. Sci.* **97,** 6640–6645 CrossRef Medline